mater.scichina.com link.springer.com

Published online 10 August 2020 | https://doi.org/10.1007/s40843-020-1392-5
Sci China Mater 2021, 64(2): 460–473

Biocompatibility and bone regeneration of PEO/Mg-Al LDH-coated pure Mg: an *in vitro* and *in vivo* study

Jie Wang[1†], Feng Peng[2,3†], Xiaolin Wu[1], Donghui Wang[2], Ao Zheng[1], Lingyan Cao[1], Chunhua Yu[1], Xuanyong Liu[2*] and Xinquan Jiang[1*]

ABSTRACT **Forming a stable anti-corrosion surface layer on magnesium (Mg) and its alloys has become a major challenge in developing a desirable degradable medical implant in bone. In this study, a porous MgO layer was first formed on Mg by plasma electrolytic oxidation (PEO), and then a Mg-Al layered double hydroxide (LDH) layer was prepared to seal the porous structure of the PEO layer (LDH-2h and LDH-12h) *via* hydrothermal treatment. The bilayer structure composite coating, which can effectively resist the penetration of surrounding media, is similar to plain Chinese tiles. The *in vitro* results revealed that compared with other coatings, the LDH-12h composite coating can reduce the release of Mg ions and induce a milder change in pH when immersed in phosphate-buffered saline (PBS). *In vitro* rat bone marrow stem cell (rBMSC) culture suggested that the LDH-12h composite coating is favorable for cell activity, proliferation and could improve the osteogenic activity of rBMSCs. A subcutaneous implantation test revealed that the as-prepared sample showed enhanced corrosion resistance and histocompatibility *in vivo*, especially in the LDH-12h group. Moreover, LDH-12h had the lowest rate of degradation and the closest combination with the new bone after being inserted into a rat femur for 12 weeks with no major organ dysfunction. In summary, the as-prepared PEO/Mg-Al LDH composite coating is able to improve the corrosion resistance and biocompatibility of Mg and to enhance osteogenic activity *in vivo*, suggesting its promising prospects for orthopedic applications.**

Keywords: plasma electrolytic oxidization, layered double hydroxide, magnesium, corrosion resistance, bone repair

INTRODUCTION

Traditional inert metal biomaterials, such as stainless steel, cobalt-chromium alloy, titanium and its alloys, are widely used in orthopedic implants [1–3]. Nevertheless, their elastic modulus is far more than that of natural bone tissue, resulting in a stress shielding effect and insufficient bone regeneration [4]. In addition, when the bone is healed, patients need a second surgery to remove the implanted materials, which would increase their economic and mental pressure [5]. Therefore, magnesium (Mg) and its alloys have attracted increasing attention for their biodegradability and suitable elastic modulus [6–9]. In fact, the application of Mg in the biomedical field can be traced back to 140 years ago. Huse [10] first used Mg wire to suture vascular lesions in 1878. However, it was not until 2013 that an Mg-based implant product received its first certification, namely, CE certification [8]. The main obstacle to its clinical application is its fast degradation rate *in vivo*, which would lead to the formation of a gas cavity and local alkalization around the implants. For load-bearing implants, fast degradation would also result in the rapid decline of mechanical support capacity and thus clinical failure [11–13]. Hence, improving the corrosion resistance of Mg implants is of great importance.

Surface modification strategies, including hydrothermal treatment [14], plasma electrolytic oxidation (PEO) [15,16], electrophoretic deposition [17,18], spray coating [19], and chemical conversion coating [20], are effective methods to improve the corrosion resistance of Mg and

[1] Department of Prosthodontics, Shanghai Engineering Research Center of Advanced Dental Technology and Materials, Shanghai Key Laboratory of Stomatology & Shanghai Research Institute of Stomatology, National Clinical Research Center for Oral Diseases, Shanghai Ninth People's Hospital, College of Stomatology, Shanghai Jiao Tong University School of Medicine, Shanghai 200011, China
[2] State Key Laboratory of High Performance Ceramics and Superfine Microstructure, Shanghai Institute of Ceramics, Chinese Academy of Sciences, Shanghai 200050, China
[3] Department of Orthopedics, Guangdong Provincial People's Hospital, Guangdong Academy of Medical Sciences, Guangzhou 510080, China
[†] These authors contributed equally to this work.
[*] Corresponding authors (emails: xyliu@mail.sic.ac.cn (Liu X); xinquanj@aliyun.com (Jiang X))

its alloys with controllable coating thickness and phase composition. Among these methods, PEO is most studied because of its high hardness and strong adhesion, as well as favorable corrosion protection [21–24]. Nevertheless, the porous structure of the PEO coating is a disadvantage in terms of its long-term protection because a corrosive liquid could penetrate into the substrate [16,25]. Mg-Al layered double hydroxide (LDH) is a plain tile-like structure generated *in situ* on PEO by many methods such as hydrothermal treatment, urea hydrolysis, and steam coating [26]. The plain tile-like structure has been used on the roofs of building for thousands of years and has successfully been proven effective in preventing penetration. In our previous study, we fabricated LDH tiles to seal the porous PEO coating (PEO/LDH) on AZ31 to enhance its corrosion resistance and biocompatibility [27]. After modification with the PEO/LDH bilayer coating, rat bone marrow stem cells (rBMSCs) showed good activity on its surface, even when cultured for 14 d. Nevertheless, the study lacked an *in vivo* evaluation. Because there are great differences between the *in vitro* and *in vivo* environments, it is necessary to assess the corrosion behavior and bone regeneration of the PEO/LDH bilayer *via* animal experiments. On the other hand, studies revealed that Al is potentially related to neurotoxicity [28–30]. Consequently, AZ31 was abandoned in this work, and pure Mg was chosen as the substrate.

In theory, the longer the processing time is, the thicker the tile-like LDH layer, and the better the anticorrosion effect [31]. However, few studies have considered PEO/LDH-modified pure Mg *in vivo* with different thicknesses of the LDH layer. Moreover, the degradation products and degradation rate of the Mg implant would influence the peri-implant microenvironment and tissue response. Fast Mg degradation with the accumulation of hydrogen could cause adverse host reactions, which is a disadvantage for osseointegration [32,33]. The degradation products of Mg-based biomaterials such as magnesium content [25,34] and the evolved gases [35] would alter the local host reaction and subsequently influence the bone repair effect. Some Mg degradation products such as Mg ion could enter and flow with the bloodstream to reach distant organ tissues and cause damage to them. Systematic evaluation of this novel PEO/LDH-coated pure Mg *in vivo* is essential.

With the above considerations in mind, in this study, a PEO and Mg-Al LDH bilayer coating were fabricated on pure Mg by PEO and hydrothermal treatment. Mg-Al LDH layers with different thicknesses fully sealed the porous structure of the PEO coating in a similar manner to traditional plain Chinese tiles. Samples were inserted in subcutaneous tissue and femur to evaluate their corrosion behavior and biocompatibility. Peri-implant new bone tissue was analyzed by a micro computed tomography (micro-CT) assay and histomorphometric analysis for assessment of bone healing ability. Finally, systemic host responses (serum ion concentrations, subcutaneous inflammatory response and histological manifestation of important organs) to the Mg degradation products were also monitored.

EXPERIMENTAL SECTION

Sample preparation and characterization

Commercially pure Mg (>99.95 wt%) bought from Suzhou Rongqian Rare Metal Products Co., Ltd. (China) was cut into samples with different sizes: 10 mm in diameter and 2 mm in thickness for *in vitro* study, 6 mm in diameter and 2 mm in thickness for subcutaneous implantation, and 2 mm in diameter and 10 mm in height for bone implantation. The samples were sonically cleaned in ethyl alcohol (Sinopharm, China) and kept in ethyl alcohol before utilization. The PEO process was performed on pure Mg as previously reported [36]. In detail, 4 L of solution containing 0.04 mol L^{-1} $Na_2SiO_3 \cdot 9H_2O$, 0.1 mol L^{-1} KOH and 0.2 mol L^{-1} $KF \cdot 2H_2O$ (Sinopharm, China) was used as the electrolyte. The PEO process was conducted by using PEO equipment (Southwestern Institute of Physics, China) with a constant current of 0.8 A, a frequency of 800 Hz and a 10% duty cycle. The process was stopped at 360 V, and the obtained samples were rinsed with deionized water and denoted by PEO.

To seal the pores in the PEO coating, hydrothermal treatment was applied to the PEO samples. As our previous study, they were placed in a Teflon-lined stainless steel autoclave, and then a hydrothermal solution containing 0.02 mol L^{-1} $Al(NO_3)_3$ (pH value was adjusted to 12.8 by NaOH) was added [37]. After reacting at 120°C for 2 and 12 h, the obtained samples were rinsed with deionized water and denoted as LDH-2h and LDH-12h, respectively.

The surface and cross-sectional morphology of the Mg, PEO, LDH-2h and LDH-12h groups were observed through scanning electron microscopy (SEM; Hitachi-3400, Japan). For the preparation of cross-sectional specimens, two specimens were clamped by face to face, and then immersed in resin. After the resin was solidified, the resin was polished by 200# and 1000# SiC paper until the

cross-section of the specimens were exposed. The phase compositions of the Mg, PEO, LDH-2h and LDH-12h samples were detected *via* X-ray diffraction (XRD; D/Max, RIGAKU, Japan).

Ions release and pH value change

Mg, PEO, LDH-2h and LDH-12h samples were placed in a 24-well plate, and then 1 mL of alpha-minimum essential medium (α-MEM, Gibco, Invitrogen Inc., USA) was added. The plate was placed at 37°C in a 5% CO_2 incubator. After 1 d, the extract was collected and added to 1 mL of fresh α-MEM described as cell medium (CM). The process was repeated six times. On the 7^{th} day, the Mg^{2+} concentration, Al^{3+} concentration and pH value of all the extracts were measured *via* an inductively coupled plasma optical emission spectrometer (ICP-OES, Varian Liberty 150, USA) and a pH meter (METTLER TOLEDO, USA), respectively.

***In vitro* evaluation**

In vitro cell morphology

The samples were sterilized under ultraviolet radiation for 12 h and then placed in a 24-well plate. An rBMSC suspension (1 mL) was added to the plate at a density of 5×10^4 cells per well. α-MEM containing 10% fetal bovine serum (FBS; HyClone, USA) and 1% antimicrobial penicillin/streptomycin mixture (P/S; HyClone, USA) was used as culture medium, and the cells were cultured at 37°C in a 5% CO_2 incubator. After culturing for 1, 2 and 3 d, the samples were gently rinsed with phosphate-buffered saline (PBS) and immersed in 2.5 vol% glutaraldehyde. Subsequently, the cells were dehydrated in graded ethanol (30%, 50%, 75%, 90%, 95% and 100%), dried in hexamethyldisilazane ethanol solution, and observed by SEM.

In vitro cell proliferation

After sterilization by ultraviolet irradiation, all the samples were immersed in CM for 24 h. The sample area-extraction medium ratio was 2 cm^2/1 mL. The extracted solution was designated as 100% and then diluted to 50% and 25% with CM. Then, 100 μL of cell suspension with a density of 5×10^4 cells mL^{-1} was added to a 96-well culture plate. After 24 h of incubation, the rBMSCs were exposed to the extracted solution at different concentrations for 24, 48 or 72 h. The number of cells was tested by cell counting kit-8 solution (CCK-8; Dojindo Laboratories Inc., Japan) according to the manufacturer's instructions.

ALP activity assay

The rBMSCs were seeded in 12-well tissue culture plates to study the influence of the extracted solutions at different concentrations on their osteogenic capacity for 72 h. Alkaline phosphatase (ALP) activity was visualized using a BCIP/NBT alkaline phosphatase color development kit (Beyotime, China) according to the manufacturer's instructions. At the same time point, an ALP semiquantitative assay was performed as described previously [38].

***In vivo* evaluation**

Animals and surgery

Thirty-two adult male Sprague Dawley (SD) rats were purchased from the Ninth People's Hospital Animal Center (Shanghai, China). Twelve rats underwent subcutaneous implantation, and twenty rats underwent femur insertion. All procedures were conducted under animal care protocols approved by the Animal Research Committee of the Ninth People's Hospital affiliated to Shanghai Jiao Tong University. The rats were randomly divided to four experimental groups with n=4 for each group at each time point. The rats were anesthetized by intraperitoneal injection of ketamine. For subcutaneous implantation, four parallel incisions were made on the back of the rat, and each sample was inserted subcutaneously into each incision. After the rats were housed for 10, 20 or 40 d, they were euthanized, and the samples along with the surrounding subcutaneous tissue were collected for histological examination. For femur insertion, a cylindrical hole measuring approximately 2 mm in diameter was drilled along the long axis of left femur after the hind limbs were shaved, and the cylindrical implants with 2 mm in diameter and 10 mm in length were placed into each rat. In this study, twenty rats were randomly divided into five groups, with one group without implantation used as a control. After 12 weeks, all the animals were harvested, providing four samples for each group.

Sequential fluorescent labeling

A polychrome sequential fluorescent labeling method was used to visualize the process of new bone formation and mineralization. At 3, 6, and 9 weeks after surgery, 25 mg kg^{-1} tetracycline hydrochloride (Sigma, USA), 30 mg kg^{-1} alizarin red S (Sigma, USA), and 20 mg kg^{-1} calcein (Sigma, USA) were intraperitoneally administered.

Surface morphology and histological analysis

For subcutaneous implantation, the samples together with the surrounding subcutaneous tissue were harvested with scissors and scalpels. The collected samples were fixed in 4% paraformaldehyde overnight. All the implants were then carefully stripped from the surrounding tissues. The implants were scanned with SEM, and the corresponding surrounding tissues were embedded in paraffin wax. For each sample, 6 μm sections were cut off and mounted onto glass slide for hematoxylin & eosin (H&E) staining. Images were obtained and analyzed with a Motic easy scan digital slide scanner (MOTIC, China).

Blood test and visceral section

For the femur insertion group, blood samples were collected at 12 weeks. Serum inorganic salt ions such as sodium (Na), Mg, potassium (K), calcium (Ca) and phosphate (P); blood alanine aminotransferase (ALT) and aspartate aminotransferase (AST); and serum creatinine (SCr) and blood urea nitrogen (BUN), were tested by enzyme-linked immunosorbent assay (ELISA) to determine the biocompatibility of the Mg implants. In addition, patches of tissues were removed from the heart, liver, lung and kidney, and fixed in buffered formalin for H&E staining.

Micro-CT assay

After 12 weeks, the left femur with implant was harvested and fixed in 4% paraformaldehyde for 24 h. Then the samples were imaged by micro-CT (SkyScan 1176, Bruker, USA) to analyze the newly formed bone and degradation rate of the implant. The scanning parameters were set according to our previous study [39]. The volumes of the bone around the implant and the implant itself were determined using DataViewer software (SkyScan) and the CTAn program (SkyScan).

Histomorphometric observation

The left femur with implant of each group was dehydrated by ascending graded ethanol (30%, 50%, 75%, 90%, 95% and 100%) and embedded in polymethylmethacrylate (PMMA). The embedded samples were prepared in our previous study and observed by a confocal laser scanning microscope (Leica SP8, Hamburg, Germany) [40]. The same sections were counterstained with van Gieson's (VG) solution to visualize the mineralized bone tissue (red) and then scanned by SEM. Histomorphometric analysis was performed on the same slides of each group to evaluate the percentage of bone implant contact (BIC). The images were analyzed using Image-Pro Plus 6.0 software. Afterwards, the implant sample residual rate was calculated with the following formula: implant sample residual rate=(residual sample volume/initial sample volume)×100%.

Statistical analysis

Experiments were conducted with at least three samples for three independent times. All the data were expressed as the mean±standard deviation (SD). The data were analyzed using Graph-Pad Prism 5 (GraphPad, USA) and the statistically significant differences (p) between groups were identified using one-way analysis of the variance and Tukey's multiple comparison tests. Probability values of <0.05 were considered significant. The differences were expressed at * p<0.05, ** p<0.01 and *** p<0.001.

RESULTS AND DISCUSSION

Materials characterization

Fig. 1 shows the surface morphologies of all the samples. The surface of the untreated Mg was relatively flat (Fig. 1a), while numerous uniformly distributed porous structures were observed on the PEO sample (Fig. 1b). After hydrothermal treatment for 2 h, the pore structures were almost sealed by micro-/nanosheets; however, some regions were not covered by the sheets, and an obvious PEO-structure was observed (Fig. 1c). For the LDH-12h sample, the pore structures were completely sealed by micro/nanosheets, and the surface was completely covered with the sheets (Fig. 1d). Furthermore, it should be noted that the sheets on the LDH-12h sample were larger than those on the LDH-2h sample, which suggests that the sheet size grows with the hydrothermal treatment time. Fig. 2a–c display the cross-sections of the PEO,

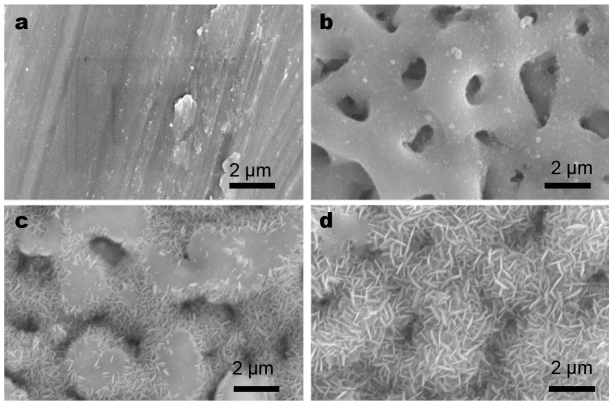

Figure 1 Surface morphologies of Mg (a), PEO (b), LDH-2h (c) and LDH-12h (d).

LDH-2h and LDH-12h coatings. The thickness of the PEO coating was approximately 5.12±0.37 μm. Moreover, the LDH-2h and LDH-12h coatings clearly exhibited bi-layer structures. The thicknesses of the inner and outer layers of the LDH-2h coating were 4.45±0.55 μm and 2.32 ±0.08 μm, respectively, and for the LDH-12h coating, the inner and outer layer thicknesses were 2.93±0.13 μm and 3.47±0.07 μm, respectively. It can be concluded that with increasing hydrothermal treatment time, the PEO layer became thinner, indicating that the PEO layer was partially dissolved during the hydrothermal treatment, and the LDH layer became thicker, suggesting that more sheets grew on the PEO layer. XRD patterns of the Mg, PEO, LDH-2h and LDH-12h samples are shown in Fig. 2d. Only Mg characteristic peaks were detected for the Mg sample. In the XRD pattern of the PEO sample, a characteristic peak of MgO was observed at approximately 42°. After hydrothermal treatment, new peaks appeared at 11.7°, indicating the formation of Mg-Al LDH. Notably, for all PEO treated samples, a feature peak was detected at 41°, which represented Mg_2SiO_4 phase formed during the oxidation process.

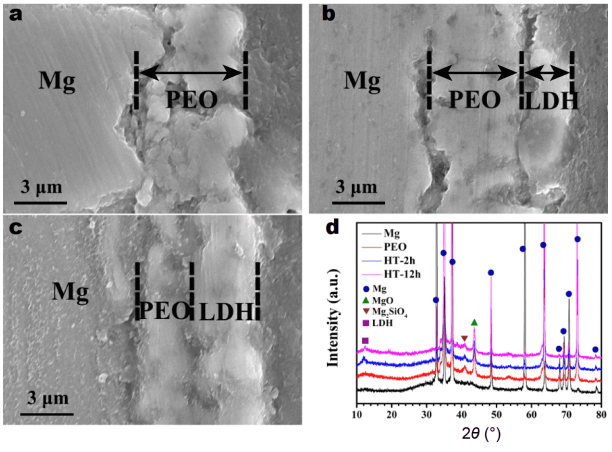

Figure 2 The morphologies of cross-section in PEO (a), LDH-2h (b) and LDH-12h (c). (d) XRD patterns of Mg, PEO, LDH-2h and LDH-12h samples.

In vitro degradation, biocompatibility and osteogenesis ability

Fig. 3a shows the changes in Mg^{2+} concentration in the extracts over a period of 7 d. The release of Mg^{2+} from all the substrates gradually decreased during the initial 3 d, and then stable release behavior was observed. At each tested time, the Mg^{2+} concentration in the extract of the Mg sample was the highest among all four tested samples, followed by the extracts of the PEO, LDH-2h and LDH-12h samples. Aluminum has long been reported to alter blood-brain barrier and has an adverse impact on the central nervous system (CNS). The tolerable weekly intake (TWI) set by the European Food Safety Authority (EFSA) is 1 mg aluminum/kg body weight (BW) in a 60-kg adult [41]. However, Al^{3+} was not detected in all samples due to the measurement range of the instrument, implying a very low Al^{3+} release in Mg-Al LDH coating. Fig. 3b shows the changes in the pH values of the extracts. All samples cause alkalization of α-MEM. However, compared with the Mg sample, all other treated samples showed a milder influence on the pH value. Among the four samples, the extract of the LDH-12h sample showed the lowest pH value during the initial 3 d, and its pH value was the same as that of the LDH-2h sample in the last 4 d. According to our previous study, 5 mmol L^{-1} Mg^{2+} is optimal for constructing an osteogenic microenvironment [42]. These results indicate that the LDH-12h sample has the best corrosion resistance and biological performance.

Cells are sensitive to factors in the surrounding microenvironment. The active chemical reaction of mag-

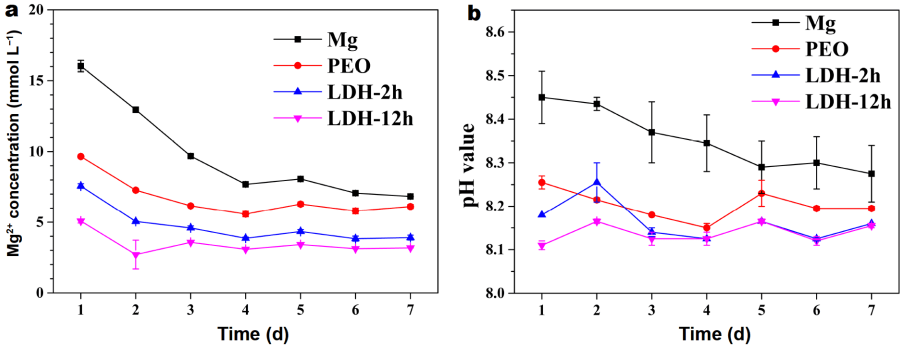

Figure 3 Mg^{2+} concentrations (a) and pH values (b) of the Mg, PEO, LDH-2h and LDH-12h extracts. The samples were immersed in α-MEM, and the extracts were collected each day.

nesium degradation on the sample surfaces would prevent cell survival. Magnesium would corrode continuously in solutions containing chloride ions, producing hydrogen and magnesium hydroxide [43]. The LDH groups which effectively resist the penetration of surrounding media would provide a relatively inert environment for cell activity theoretically. In this study, to evaluate the effect of the as-prepared samples on cell viability, the cells were cultured on sample surfaces and in sample extracts, respectively. Fig. 4 shows the morphology of rBMSCs after culture on various samples. No cells were observed on the Mg and PEO samples. For the LDH-2h sample, only a few cells were observed while many cells adhered to the surface of the LDH-12h sample after culturing for 1 d. Furthermore, all the surfaces of the four samples showed cracks at day 1 (Fig. S1), indicating that liquid could permeate into the substrate, and then Mg ions would release from the substrate. With the prolongation of culture time, more cells were observed on its surface, and the cells showed a more spread morphology. These results suggest that the LDH-12 sample is better for cell adhesion, spreading and proliferation, which is consistent with the results of our previous study [27].

Fig. 5a shows the viability of rBMSCs in extracts with different concentrations for three consecutive days. All cells in the extracts of the pure Mg and PEO samples completely died (<15%) at all periods. However, when the extracts were diluted to 50% and 25%, the cytotoxicity was largely mitigated. On the other hand, the viabilities of cells in the LDH-2h and LDH-12h extracts were mostly

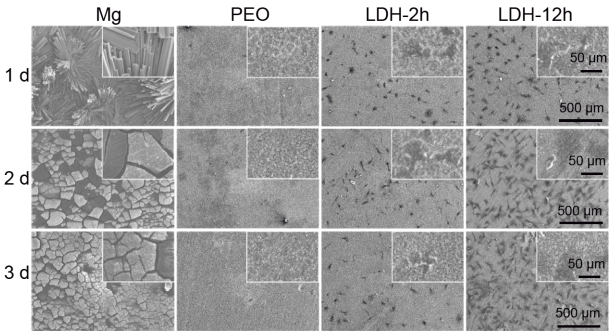

Figure 4 Morphologies of rBMSCs after culture on Mg, PEO, LDH-2h and LDH-12h for 1, 2 and 3 d.

more than 60%, suggesting slight cytotoxicity, especially in the extract of LDH-12h group, which showed more than 90% cell viability at all periods and all concentrations. Notably, the cytotoxicity of all extracts is reduced after dilution except for LDH-12h, which presents a slight difference in cytotoxicity among different concentrations. The results may be explained by the differences in Mg^{2+} concentration and pH value among the extracts. In our previous work, we found that cell viability decreased significantly when the Mg^{2+} concentration exceeded 20 mmol L^{-1} [42]. The high pH value of the Mg extracts in this experiment may also contribute to their severe cytotoxicity. Fig. 5b, c show that among the four extracts, LDH-12h had the most intense ALP staining and activity, and there was an increasing trend in the osteogenic activity of rBMSCs as the dilution of the extracts was increased. Further *in vitro* studies are needed to

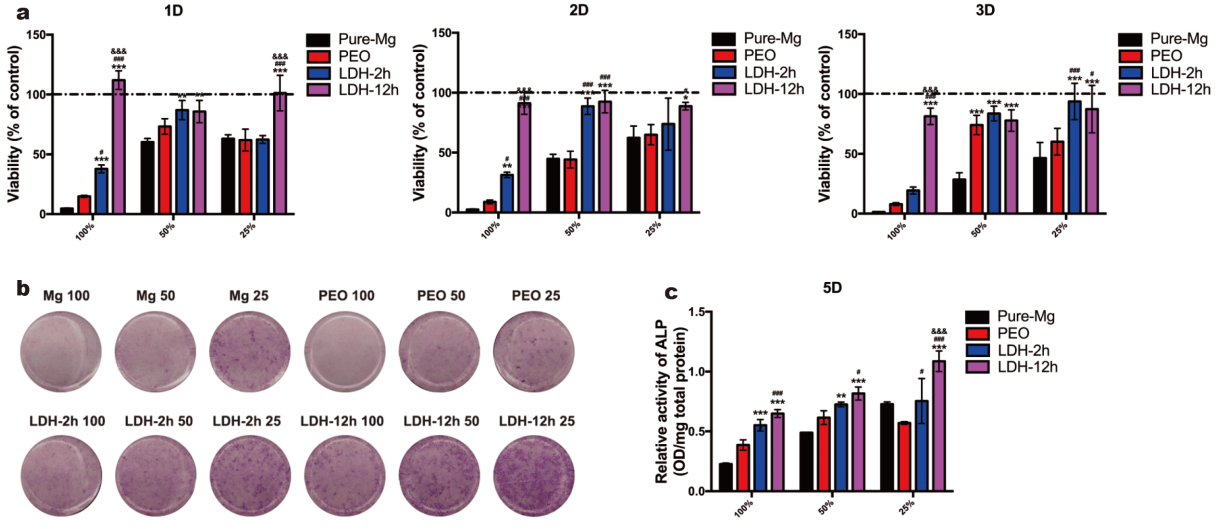

Figure 5 Cell viability (a), ALP staining (b) and ALP activity (c) of rBMSCs incubated with different concentration extracts of Mg, PEO, LDH-2h and LDH-12h samples.

demonstrate the osteogenetic effect of LDH-12h and the underlying mechanism.

All the above *in vitro* results suggest that PEO/LDH-12h coating greatly improve the degradation rate of the substrate, whether for the pure Mg in our study or AZ31 in others [44,45]. However, there are some differences in the *in vitro* biocompatibility results of these studies due to the difference in the manufacturers of base substrates and the cells (cell lines like MC3T3 [44,46,47] or primary cells like rBMSCs [45]) used. For example, the pH value of the simulated body fluid (SBF) solution containing bare AZ31 in the first day is about 7.86 in one study [47] and 8.38 in another [46]. Therefore, the *in vivo* test is needed to evaluate the effect of modification.

In vivo evaluation

Many studies show the difference of corrosive condition between *in vivo* and *in vitro* [14,48,49]. Whether the corrosion protection effect of the PEO/Mg-Al LDH composite coating would work *in vivo* is unknown. Considering different tissue systems, *in vivo* tests were carried out by short-time subcutaneous implantation and long-term femur implantation.

Subcutaneous implantation

Only the subcutaneous tissues attached to the samples were collected and analyzed. H&E-stained images of the subcutaneous capsule are shown in Fig. 6. Local tissue reaction was triggered by all samples at 10 d and gradually eased over time. This behavior could be explained by the host self-healing ability [50]. Among the four samples, LDH-12h presented the mildest inflammation reactions at all periods, as indicated by the lowest number of neutrophils (denoted by the green arrow). This phenomenon suggested that LDH-12h possessed the best histocompatibility *in vivo*. Fig. S2 shows the neutrophil density in the tissue surrounding the implants. Neutrophil density in LDH-12 was significantly less than that in the other samples at all periods, and it seemed that the inflammatory response gradually decreased in the order of Mg, PEO and LDH-2h, although the difference was not significant.

The surface condition of the samples after subcutaneous embedding was scanned by SEM. It could be found that corrosion increased over time in groups, with more and wider cracks observed in Fig. 7 (yellow arrows). Compared with those of Mg and PEO, the corrosion degrees of LDH-2h and LDH-12h were obviously milder at all time points, and corrosion was barely observed in LDH-12h at day 10 and day 20. At day 40, there were only a few small cracks on the surface of LDH-12h. This result indicated that the introduction of Mg-Al LDH onto the PEO layer provided long-term protection from corrosion *in vivo*. Furthermore, there was no tissue covering the Mg sample, while tissue residues were observed in the other three groups, especially LDH-12h (indicated by red asterisks), which implied that LDH-2h and LDH-12h produced less gas production and had better tissue affinity than the other two samples.

According to the corrosion morphology in subcutaneous (Fig. 7) and *in vitro* (Fig. 4), the corrosion mechanism of the three coatings can be presented as follows. For the bare PEO coating, the liquid could easily permeate into the substrate through the pores, as well as

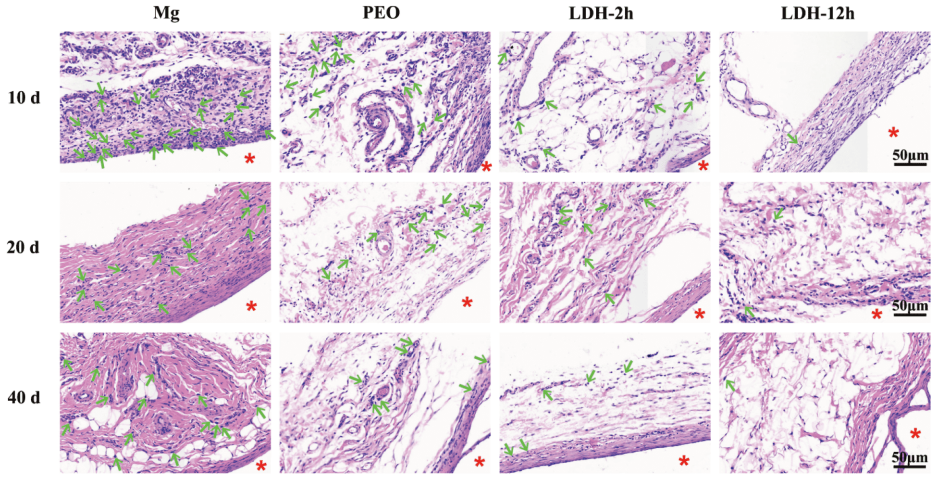

Figure 6 Photomicrographs of histological sections of Mg, PEO, LDH-2h and LDH-12h after subcutaneous implantation for 10, 20, and 40 d. The red asterisk represents the sample, and the green arrow indicates neutrophils.

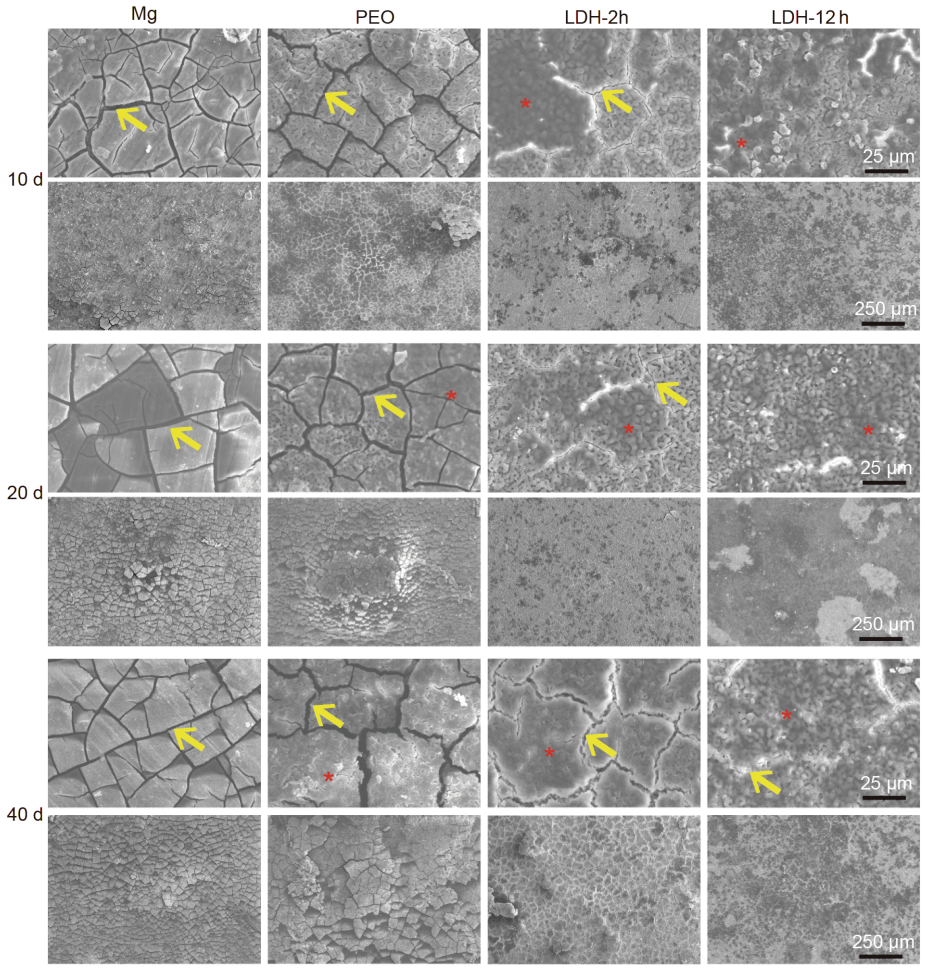

Figure 7 Surface morphologies of Mg, PEO, LDH-2h and LDH-12h after subcutaneous implantation for 10, 20, and 40 d. The yellow arrows indicate surface cracks, and the red asterisks represent the tissue residues.

induce crack inside the pores. In addition, the PEO coating is brittle, and once a tiny crack appears on the coating, it would expand rapidly. Therefore, many cracks were observed on PEO surface after being immersed in α-MEM culture medium for 1 d (Fig. 4) or subcutaneously implanted for 10 d (Fig. 7). For the LDH-2h sample, the pores of PEO layer were filled with LDH structures (Fig. 1). Thus, fewer liquid can permeate into the pores, and few cracks were formed when immersed in cultured medium or implanted subcutaneously. For the LDH-12h sample, not only the pores of PEO layer were totally filled, but also the top of the PEO layer was covered by an LDH layer, which can sufficiently inhibit the permeation of liquid. Moreover, the LDH layer can inhibit the prolongation of corrosion crack on the PEO layer. Therefore, almost no obvious cracks were observed on LDH-12h even after subcutaneous implantation for 40 d (Fig. 7).

Femur insertion

After 12 weeks, the left femurs with implants were collected and analyzed. As shown in the representative images, significant metal loss is present in the Mg and PEO groups (the white arrows in Fig. 8a show the metal loss area, and the red asterisks show the remaining metal). This result confirmed the findings in the previous study on the degradation rate *in vitro* and in subcutaneous implantations. Moreover, a deposition layer with a similar density to bone tissue was overlaid on the surface of the implant (Fig. 8a, purple triangle), especially the LDH-12h implant. This layer may be calcium phosphate deposits (hydroxyapatite, HA) and may benefit subsequent bone repair according to previous studies

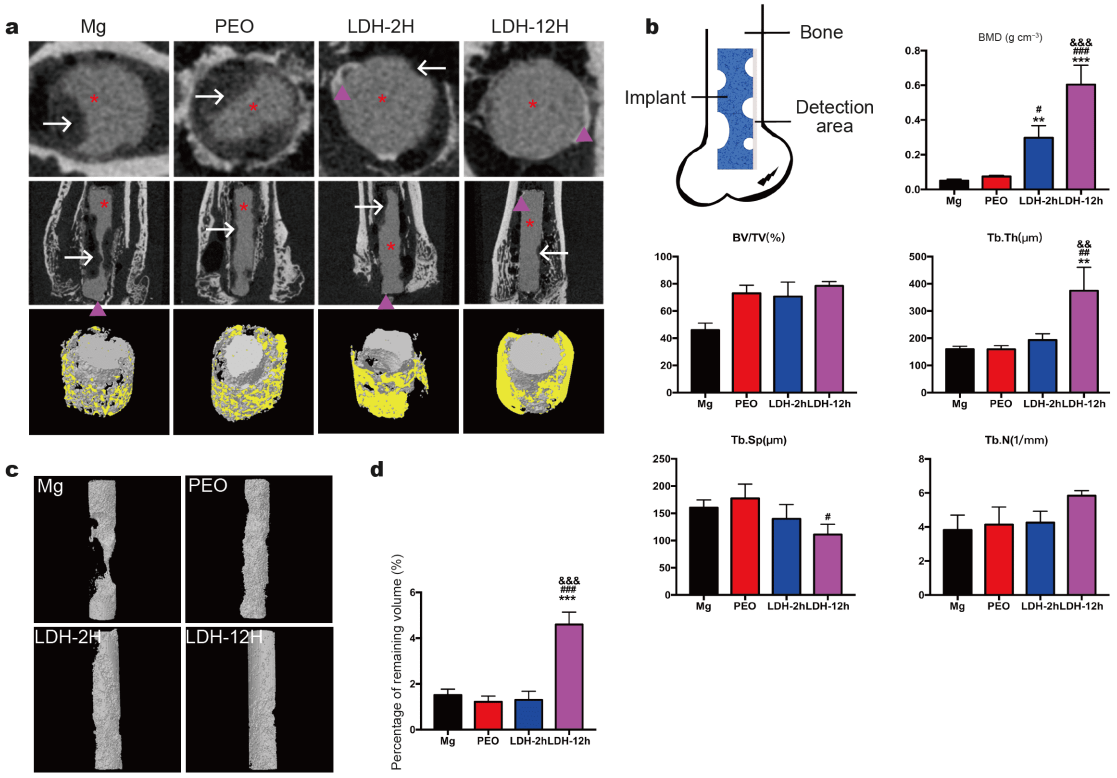

Figure 8 (a) Micro-CT analysis of Mg, PEO, LDH-2h and LDH-12h after femur implantation for 12 weeks. Representative horizontal and vertical sections and 3D reconstruction images of the peri-implant region are shown. The white arrows show the degradation position, and the red asterisks show the remaining metal. The purple triangles indicate the deposition layer with a similar density to natural bone on the surface of the implant. (b) Trabecular bone parameters of the region of interest (ROI) around the implant: trabecular BMD, BV/TV, Tb.Th, Tb.Sp and Tb.N were quantified. Representative 3D reconstruction images of the implants (c) and the percentages of remaining volume (%) of Mg, PEO, LDH-2h and LDH-12h implants after femur implantations for 12 weeks relative to the original volume before implantation (d).

[11,12,51]. On the other hand, this HA layer may slow the Mg degradation rate. Furthermore, implant osseointegration was estimated by micro-CT analysis. There were no significant differences in bone volume/tissue volume (BV/TV), trabecular separation (Tb.Sp) and trabecular number (Tb.N) among all the samples. However, compared with the other three groups, the LDH-12h treatment group exhibited a significant increase in the trabecular bone mineral density (BMD), trabecular thickness (Tb.Th) and Tb.Sp around the peri-implant region ($p<0.001$, $p<0.01$ and $p<0.05$, respectively), as shown in Fig. 8b. Although there was no significant difference among the other three groups, the pure Mg group appeared to show the least new bone formation, which may be due to the excessive hydrogen release and pH change [50,52]. Suitable degradation rates of Mg and its alloys primarily determine their persistent mechanical strengths [53].

The samples will definitely experience coating exfoliation and substrate exposure *in vivo*. For example, LDH groups experienced LDH coating breakage, PEO coating breakage, and internal pure magnesium metal exposure. Further study is needed to verify the specific form of exfoliation of the composite coating. Exposure of the magnesium would cause continuous degradation of the implant. Fig. 8c shows the three-dimensional (3D) morphology of the implants in rat femurs, and compared with the other three samples, LDH-12h displays a significantly higher residential metal volume and approximately 67.96%±4.40% of the initial material volume (Fig. 8d). Mg, PEO, and LDH-2h display 40.20%±3.79%, 40.84%±1.34% and 50.92%±6.51% of the initial material volumes, respectively. The coatings on the implant did degrade mostly or even completely but the remaining Mg base could provide some support for the bones. Considering that it is usually takes at least three months for the bone healing, improved corrosion resistance of Mg implants not only benefits biological reactions but also provides sufficient mechanical strength for the new bone during the initial fracture healing period.

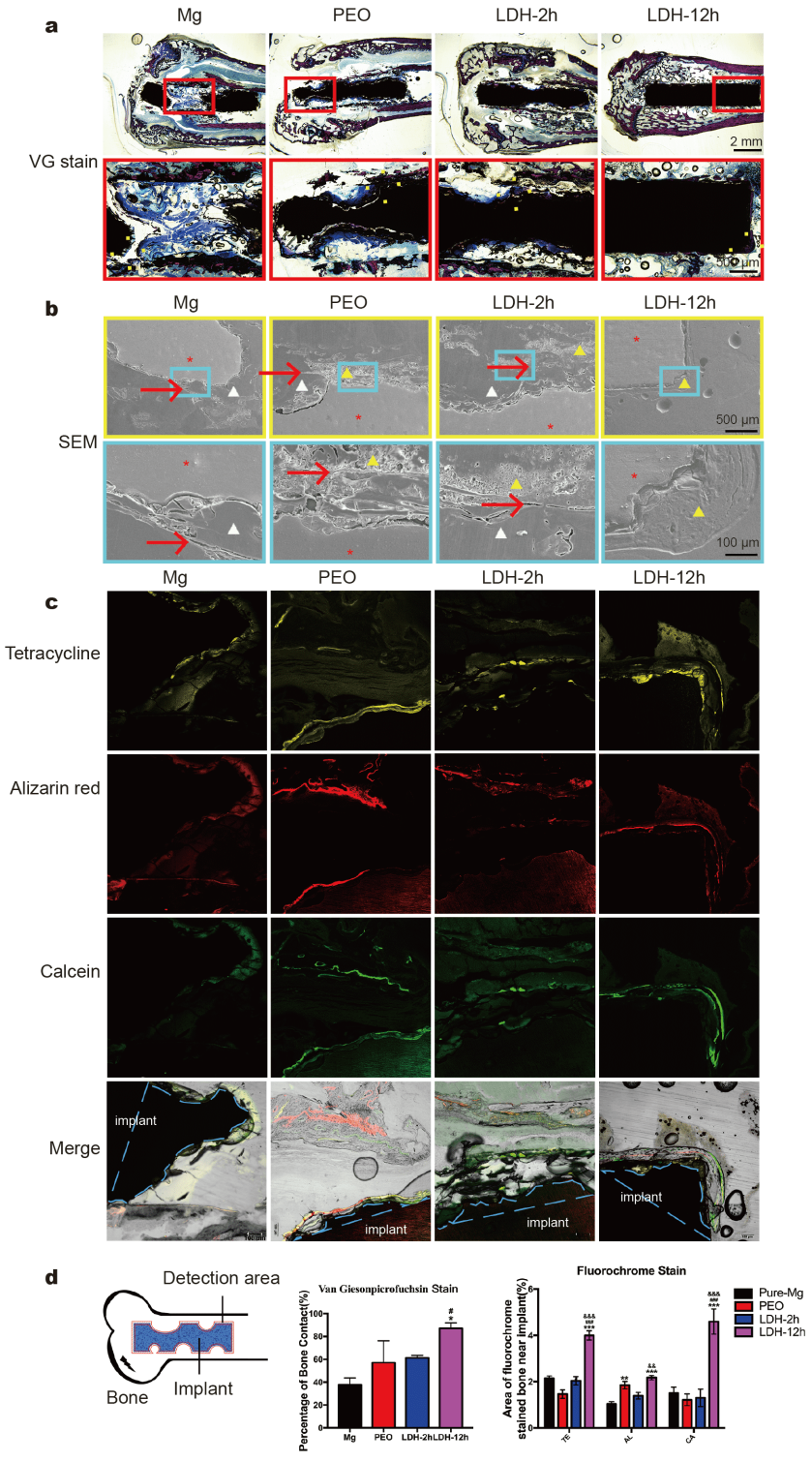

Figure 9 Histological images (a), SEM observations (b) and sequential fluorescent labeling (c) of Mg, PEO, LDH-2h and LDH-12h after femur implantation for 12 weeks. Images are shown at graded magnifications. Images of the red, yellow and blue marked areas are magnified at 40×, 50× and 250×, respectively. The white triangle shows the gap between the implant and the surrounding tissue, and the red arrows show the original implant edge. The red asterisks represent the implant, and the yellow triangles represent the new bone. (d) Quantitative analyses of the area of new bone formation around the implants by VG and sequential fluorochrome staining.

Fig. 9a, b show the histological views of VG staining and the corresponding SEM observations, respectively. In the SEM images, the white triangle denotes the gap between the degraded metal and the bone tissue, and the red arrows show the original implant edge (Fig. 9b). It can be seen that some gap exists between the new bone and Mg implant for the Mg group, indicating that the new bone could not respond in a suitable manner to pure Mg degradation. For the PEO and LDH-2h implants, the gap and new bone were found to exist simultaneously around the material. By contrast, in the LDH-12h group, the rate of material degradation matches the rate of new bone formation, and the remaining implant is closely surrounded by new bone (the red asterisk represents the implant, and the yellow triangle represents the new bone). The sequential fluorescent labeling results (Fig. 9c) are consistent with previous data that LDH-12h group shows better osteointegration than that of the other three groups. BIC analysis by VG and sequential fluorescent staining (Fig. 9d) shows that the new bone is almost wrapped around the entire LDH-12h implant and the implant shows the most new bone formation among the four types of implant. Mg-based implants induce a proper biological response at the bone-implant interface and subsequently facilitate the bone repair. In the present study, LDH-12h shows the best biocompatibility and bone repair performance.

The gold standard to evaluate the biocompatibility is the histological response of organic tissue. The histological examination of major organs showed that there was no obvious pathological phenomenon in the heart and lung (Fig. 10). The liver structure showed that the hepatocytes in the Mg group were slightly enlarged and the structure of the hepatic sinusoids was destroyed to some extent. The hepatic sinusoids in the PEO group were also partially destroyed, while those in the two LDH groups did not change. Renal sections presented bleeding in the renal interstitial of the Mg and PEO groups; by contrast, healthy renal tissue was observed in the LDH groups, and no significant difference was observed between the two groups. However, there were no significant changes in the serum ion concentrations (Fig. 11). Mg implants did not cause metabolism disorder of major ions such as Na, Mg and Ca. There was also no significant difference in ALT, AST, BUN and SCr, the four most important biomarkers of the liver and kidney functions. The absence of organic lesions in LDH-12h proves its good biocompatible capacity. In this study, we tested the rats at only the end of 12 weeks and did not perform long-term dynamic monitoring. The fact that the serological results and tissue section results did not completely match may be ascribed to the rapid degradation of magnesium-based metals in the initial stage of implantation. The injury did emerge, but the rats could gradually repair the damage over time, whereas the tissue damage recovery was much slower. Further study on the continuous and comprehensive detection of physiological and biochemical reactions in rats is needed.

CONCLUSIONS

In summary, we successfully developed a PEO/Mg-Al LDH composite coating with a bilayer structure similar to Chinese roof tiles on the surface of pure Mg by combining PEO and hydrothermal treatment. These two structures complement each other to form an effective corrosion-resistant layer on the Mg surface. The thickness of Mg-Al LDH coating increased with the processing time and LDH-12h greatly improved its corrosion resistance

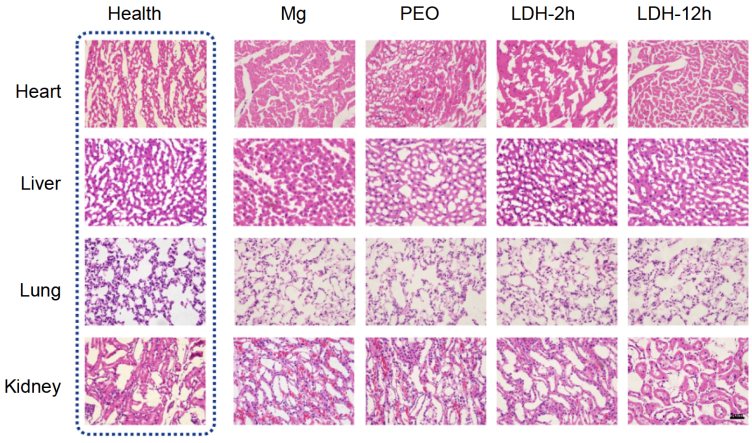

Figure 10 Histological H&E images of major organic tissues for the Mg, PEO, LDH-2h and LDH-12h groups after femur implantation for 12 weeks.

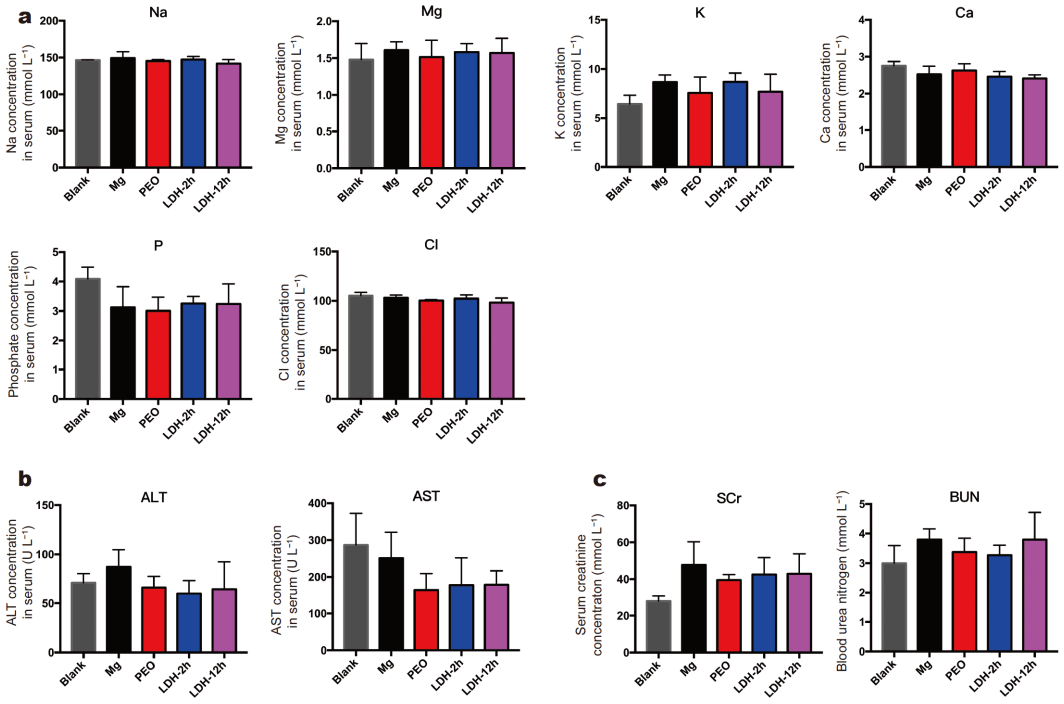

Figure 11 Levels of main serum indices in the blank, Mg, PEO, LDH-2h and LDH-12h groups after femur implantation for 12 weeks. Serum ion concentrations: (a) Na, Mg, K, Ca, P, chlorine (Cl); (b) ALT and AST; (c) SCr and BUN.

and osteogenic activity of rBMSCs *in vitro*. Moreover, the corrosion resistance and biocompatibility of LDH-12h were remarkably enhanced in both short-term subcutaneous and long-term bone implantation. And no obvious organ damage and hematological changes were found in rats after three months for the LDH groups. The flexibility of fabrication, greatly improved corrosion resistance, biocompatibility and good bioactivity *in vitro* and *in vivo* indicate that the PEO/Mg-AL LDH composite coating is promising in surface modification of biodegradable magnesium-based implants for orthopedic and dental applications.

Received 27 March 2020; accepted 12 May 2020; published online 10 August 2020

1 Fuglsig JMCS, Thorn JJ, Ingerslev J, *et al.* Long term follow-up of titanium implants installed in block-grafted areas: A systematic review. Clin Implant Dent Relat Res, 2018, 20: 1036–1046
2 Geetha M, Singh AK, Asokamani R, *et al.* Ti based biomaterials, the ultimate choice for orthopaedic implants: A review. Prog Mater Sci, 2009, 54: 397–425
3 Liu X, Chu P, Ding C. Surface modification of titanium, titanium alloys, and related materials for biomedical applications. Mater Sci Eng-R-Rep, 2004, 47: 49–121
4 Abdel-Hady Gepreel M, Niinomi M. Biocompatibility of Ti-alloys for long-term implantation. J Mech Behav Biomed Mater, 2013, 20: 407–415
5 Albrektsson T, Chrcanovic B, Molne J, *et al.* Foreign body reactions, marginal bone loss and allergies in relation to titanium implants. Euro J Oral Implantol, 2018, 11: S37–S46
6 Song MS, Zeng RC, Ding YF, *et al.* Recent advances in biodegradation controls over Mg alloys for bone fracture management: A review. J Mater Sci Tech, 2019, 35: 535–544
7 Ali M, Hussein MA, Al-Aqeeli N. Magnesium-based composites and alloys for medical applications: A review of mechanical and corrosion properties. J Alloys Compd, 2019, 792: 1162–1190
8 Windhagen H, Radtke K, Weizbauer A, *et al.* Biodegradable magnesium-based screw clinically equivalent to titanium screw in hallux valgus surgery: Short term results of the first prospective, randomized, controlled clinical pilot study. Biomed Eng Online, 2013, 12: 62
9 Witte F. The history of biodegradable magnesium implants: A review. Acta Biomater, 2010, 6: 1680–1692
10 Huse E. A new ligature. Chicago Med J Exam, 1878, 172(2)
11 Yu Y, Lu H, Sun J. Long-term *in vivo* evolution of high-purity Mg screw degradation: Local and systemic effects of Mg degradation products. Acta Biomater, 2018, 71: 215–224
12 Han P, Cheng P, Zhang S, *et al. In vitro* and *in vivo* studies on the degradation of high-purity Mg (99.99 wt%) screw with femoral intracondylar fractured rabbit model. Biomaterials, 2015, 64: 57–69
13 Chen S, Zhang J, Chen Y, *et al.* Application of phenol/amine copolymerized film modified magnesium alloys: Anticorrosion and surface biofunctionalization. ACS Appl Mater Interfaces, 2015, 7: 24510–24522
14 Peng F, Li H, Wang D, *et al.* Enhanced corrosion resistance and biocompatibility of magnesium alloy by Mg-Al-layered double

hydroxide. ACS Appl Mater Interfaces, 2016, 8: 35033–35044
15 Yin ZZ, Qi WC, Zeng RC, *et al.* Advances in coatings on biodegradable magnesium alloys. J Magnesium Alloys, 2020, 8: 42–65
16 Cui LY, Zeng RC, Guan SK, *et al.* Degradation mechanism of micro-arc oxidation coatings on biodegradable Mg-Ca alloys: The influence of porosity. J Alloys Compd, 2017, 695: 2464–2476
17 Xiong Y, Lu C, Wang C, *et al.* The *n*-MAO/EPD bio-ceramic composite coating fabricated on ZK60 magnesium alloy using combined micro-arc oxidation with electrophoretic deposition. Appl Surf Sci, 2014, 322: 230–235
18 Yang YX, Fang Z, Liu YH, *et al.* Biodegradation, hemocompatibility and covalent bonding mechanism of electrografting polyethylacrylate coating on Mg alloy for cardiovascular stent. J Mater Sci Tech, 2020, 46: 114–126
19 Gao YL, Liu Y, Song XY. Plasma-sprayed hydroxyapatite coating for improved corrosion resistance and bioactivity of magnesium alloy. J Therm Spray Tech, 2018, 27: 1381–1387
20 Duan G, Yang L, Liao S, *et al.* Designing for the chemical conversion coating with high corrosion resistance and low electrical contact resistance on AZ91D magnesium alloy. Corros Sci, 2018, 135: 197–206
21 Narayanan TSNS, Park IS, Lee MH. Strategies to improve the corrosion resistance of microarc oxidation (MAO) coated magnesium alloys for degradable implants: Prospects and challenges. Prog Mater Sci, 2014, 60: 1–71
22 Jovović J, Stojadinović S, Šišović NM, *et al.* Spectroscopic study of plasma during electrolytic oxidation of magnesium- and aluminium-alloy. J Quant Spectrosc Radiat Transfer, 2012, 113: 1928–1937
23 Zhang L, Zhang J, Chen C, *et al.* Advances in microarc oxidation coated AZ31 Mg alloys for biomedical applications. Corros Sci, 2015, 91: 7–28
24 Zhang ZQ, Wang L, Zeng MQ, *et al.* Biodegradation behavior of micro-arc oxidation coating on magnesium alloy-from a protein perspective. Bioact Mater, 2020, 5: 398–409
25 Zeng RC, Cui L, Jiang K, *et al. In vitro* corrosion and cytocompatibility of a microarc oxidation coating and poly(*L*-lactic acid) composite coating on Mg-1Li-1Ca alloy for orthopedic implants. ACS Appl Mater Interfaces, 2016, 8: 10014–10028
26 Guo L, Wu W, Zhou Y, *et al.* Layered double hydroxide coatings on magnesium alloys: A review. J Mater Sci Tech, 2018, 34: 1455–1466
27 Peng F, Wang D, Tian Y, *et al.* Sealing the pores of PEO coating with Mg-Al layered double hydroxide: Enhanced corrosion resistance, cytocompatibility and drug delivery ability. Sci Rep, 2017, 7: 8167
28 El-Rahman S. Neuropathology of aluminum toxicity in rats (glutamate and GABA impairment). Pharmacol Res, 2003, 47: 189–194
29 Kumar V, Gill KD. Aluminium neurotoxicity: Neurobehavioural and oxidative aspects. Arch Toxicol, 2009, 83: 965–978
30 Lubkowska A, Chlubek D. Aluminum in the human environment—Absorption and toxicity. Trace Elements and Electrolyt, 2015, 32: 52–59
31 Zhang G, Wu L, Tang A, *et al.* Growth behavior of MgAl-layered double hydroxide films by conversion of anodic films on magnesium alloy AZ31 and their corrosion protection. Appl Surf Sci, 2018, 456: 419–429
32 Berglund IS, Jacobs BY, Allen KD, *et al.* Peri-implant tissue response and biodegradation performance of a Mg-1.0Ca-0.5Sr alloy in rat tibia. Mater Sci Eng-C, 2016, 62: 79–85
33 Huehnerschulte TA, Angrisani N, Rittershaus D, *et al. In vivo* corrosion of two novel magnesium alloys ZEK100 and AX30 and their mechanical suitability as biodegradable implants. Materials, 2011, 4: 1144–1167
34 Yoshizawa S, Brown A, Barchowsky A, *et al.* Magnesium ion stimulation of bone marrow stromal cells enhances osteogenic activity, simulating the effect of magnesium alloy degradation. Acta Biomater, 2014, 10: 2834–2842
35 Hänzi AC, Gerber I, Schinhammer M, *et al.* On the *in vitro* and *in vivo* degradation performance and biological response of new biodegradable MgYZn alloys. Acta Biomater, 2010, 6: 1824–1833
36 Tian P, Peng F, Wang D, *et al.* Corrosion behavior and cytocompatibility of fluoride-incorporated plasma electrolytic oxidation coating on biodegradable AZ31 alloy. Regener Biomater, 2016, 4: 1–10
37 Peng F, Wang D, Zhang D, *et al.* PEO/Mg–Zn–Al LDH composite coating on Mg alloy as a Zn/Mg ion-release platform with multifunctions: Enhanced corrosion resistance, osteogenic, and antibacterial activities. ACS Biomater Sci Eng, 2018, 4: 4112–4121
38 Wang J, Qian S, Liu X, *et al.* M2 macrophages contribute to osteogenesis and angiogenesis on nanotubular TiO_2 surfaces. J Mater Chem B, 2017, 5: 3364–3376
39 Lu T, Wen J, Qian S, *et al.* Enhanced osteointegration on tantalum-implanted polyetheretherketone surface with bone-like elastic modulus. Biomaterials, 2015, 51: 173–183
40 Jiang L, Zhang W, Wei L, *et al.* Early effects of parathyroid hormone on vascularized bone regeneration and implant osseointegration in aged rats. Biomaterials, 2018, 179: 15–28
41 Klotz K, Weistenhöfer W, Neff F, *et al.* The health effects of aluminum exposure. Deutsch Aerztebl Int, 2017, 114: 653–659
42 Lin S, Yang G, Jiang F, *et al.* A magnesium-enriched 3D culture system that mimics the bone development microenvironment for vascularized bone regeneration. Adv Sci, 2019, 6: 1900209
43 Wang J, Tang J, Zhang P, *et al.* Surface modification of magnesium alloys developed for bioabsorbable orthopedic implants: A general review. J Biomed Mater Res, 2012, 100B: 1691–1701
44 Li CY, Gao L, Fan XL, *et al. In vitro* degradation and cytocompatibility of a low temperature *in-situ* grown self-healing Mg-Al LDH coating on MAO-coated magnesium alloy AZ31. Bioact Mater, 2020, 5: 364–376
45 Peng F, Zhang D, Wang D, *et al.* Enhanced corrosion resistance and biocompatibility of magnesium alloy by hydroxyapatite/graphene oxide bilayer coating. Mater Lett, 2020, 264: 127322
46 Tian P, Liu X, Ding C. *In vitro* degradation behavior and cytocompatibility of biodegradable AZ31 alloy with PEO/HT composite coating. Colloids Surf B-Biointerfaces, 2015, 128: 44–54
47 Wei Z, Tian P, Liu X, *et al. In vitro* degradation, hemolysis, and cytocompatibility of PEO/PLLA composite coating on biodegradable AZ31 alloy. J Biomed Mater Res, 2015, 103: 342–354
48 Bowen PK, Drelich A, Drelich J, *et al.* Rates of *in vivo* (arterial) and *in vitro* biocorrosion for pure magnesium. J Biomed Mater Res, 2015, 103: 341–349
49 Hiromoto S, Inoue M, Taguchi T, *et al. In vitro* and *in vivo* biocompatibility and corrosion behaviour of a bioabsorbable magnesium alloy coated with octacalcium phosphate and hydroxyapatite. Acta Biomater, 2015, 11: 520–530
50 Zhao D, Witte F, Lu F, *et al.* Current status on clinical applications of magnesium-based orthopaedic implants: A review from clinical translational perspective. Biomaterials, 2017, 112: 287–302
51 Li Z, Gu X, Lou S, *et al.* The development of binary Mg-Ca alloys

for use as biodegradable materials within bone. Biomaterials, 2008, 29: 1329–1344
52 Walker J, Shadanbaz S, Woodfield TBF, *et al.* Magnesium biomaterials for orthopedic application: A review from a biological perspective. J Biomed Mater Res, 2014, 102: 1316–1331
53 Angrisani N, Reifenrath J, Zimmermann F, *et al.* Biocompatibility and degradation of LAE442-based magnesium alloys after implantation of up to 3.5 years in a rabbit model. Acta Biomater, 2016, 44: 355–365

Acknowledgements This work was supported by the National Natural Science Foundation of China (81901048, 81921002, 81620108006 and 31771044), Shanghai Committee of Science and Technology, China (18410760600), and the International Partnership Program of Chinese Academy of Sciences (GJHZ1850).

Author contributions Jiang X, Liu X and Wang J conceived the concept of the study and provided funding support; Peng F and Wang D provided experimental materials and processing technology support; Peng F conducted the part of sample preparation and characterization experiments; Peng F and Wu X conducted the part of *in vitro* rBMSC experiments; Zheng A, Cao L, Yu C and Wang J conducted the *in vivo* experiments; Wang J and Peng F performed data analysis and drafted the manuscript; Jiang X, Liu X and Cao L reviewed the manuscript; Wang J, Jiang X, Peng F and Liu X integrated the suggestions of all authors and finished the paper.

Conflict of interest The authors declare that they have no conflict of interest.

Supplementary information Supporting data are available in the online version of the paper.

Jie Wang received her master degree of seven-year program in stomatology from Nanjing University in 2014 and PhD degree from Shanghai Jiao Tong University School of Medicine in 2017. Her research interests include tissue engineering and regenerative medicine, with a particular focus on the biodegradable materials.

Feng Peng received his bachelor degree from Central South University in 2014 and PhD degree from Shanghai Institute of Ceramics, Chinese Academy of Sciences in 2019. His current research interest focuses on biodegradable magnesium alloys for biomedical application.

Xuanyong Liu received his PhD degree in materials science and engineering from Shanghai Institute of Ceramics, Chinese Academy of Sciences, in 2002. His research interests lie in the following areas: nanosized and functionalized surface of biomedical Ti alloys, PEEK and biodegradable magnesium alloys, surface modification of biomaterials using plasma immersion ion implantation & deposition (PIII&D) technology, and plasma sprayed bioactive ceramic coatings.

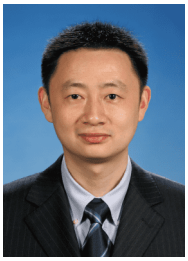

Xinquan Jiang now serves as the Executive Dean of the College of Stomatology, Shanghai Jiao Tong University, Director of the Department of Prosthodontics of Shanghai Ninth People's Hospital, Director of Shanghai Engineering and Research Center in the Universities for Advanced Dental Technology and Materials. His lab focuses on the research and application of the regeneration and repair of oral and maxillofacial bone tissues as well as expanding basic research into clinical practice.

PEO/Mg-Al LDH涂层增强金属镁的生物相容性和成骨作用: 体内外研究

王洁[1†], 彭峰[2,3†], 吴晓琳[1], 王东辉[2], 郑奥[1], 曹玲燕[1], 郁春华[1], 刘宣勇[2*], 蒋欣泉[1*]

摘要 镁(Mg)及其合金因具有生物可降解和促成骨效应而成为理想的骨内固定材料, 但其抗腐蚀能力差、体内降解快的缺点限制了其临床应用. 开发稳定的防腐涂层是镁基金属临床应用的主要挑战. 本研究首先通过等离子体电解氧化法(PEO)在Mg表面形成多孔的PEO涂层, 然后通过水热处理制备Mg-Al层状双氢氧化物(LDH)层来封闭MgO层的多孔结构(根据处理时间不同分为LDH-2h和LDH-12h组). 体外实验结果表明, 与其他涂层相比, LDH-12h组在磷酸盐缓冲液(PBS)中可以有效减少Mg^{2+}释放并抑制pH值变化. 另外, LDH-12h组促进了大鼠骨髓干细胞(rBMSC)的生物活性、增殖速率以及成骨活性. 大鼠皮下植入试验表明, 经过改性的纯镁金属在体内的耐蚀性和组织相容性增加, 尤其是LDH-12h组. 此外, LDH-12h组植入大鼠股骨12周后降解率最低、与新生骨结合最紧密, 并且未发现主要器官功能障碍. 本研究所制备的PEO/Mg-Al LDH复合涂层能够明显改善Mg的耐蚀性和生物相容性, 增强体内成骨活性, 具有良好的临床应用前景.

